

rived with the wave algorithm with an error of less than 10% if an averaged elastic property of the sea ice is used (20). The wave propagation characteristics result in a natural averaging of the ice thicknesses. Further, by averaging the directional ice thicknesses, a spatially averaged effective ice thickness is obtained (20, 21). Here we compare these ice thickness estimates (21) to MY ice area during the common observation period. Figure 2 shows the interannual variability of the mean end-of-winter (April–May) ice thickness and winter MY ice area from 1978/79 to 1990/91. The decreases are more pronounced from 1987 onward, associated with changes in atmospheric circulation (such as an increase in the frequency of low-pressure systems in the Arctic) since the late 1980s (6). The high degree of correspondence ($r \sim 0.88$, $P < 0.01$) between these independent data (which was unexpected; after all, MY ice can become substantially thinner and still count toward the MY ice area) reveals that a relationship exists between ice thickness and area. The potential importance of this observation is twofold. First, it indicates that the observed decrease in MY ice area from 1978 to 1998 represents a substantial (that is, a negative mass balance) rather than peripheral effect. Second, it suggests that the interannual variability and trends of arctic ice thickness may be estimated to a first order through an empirical relationship with MY ice area, as 77% (r^2) of the variability in ice thickness is explained by variability in MY ice area, the more readily monitored parameter. However, this relationship requires further investigation, and it is noted that the changes in effective ice thickness (21) are considerably less than those reported elsewhere (19).

The balance of evidence thus indicates an ice cover in transition, which, if continued, could lead to a markedly different ice-ocean-atmosphere regime in the Arctic. However, 20 years are inadequate to establish that this is a long-term trend rather than reflecting decadal-scale atmosphere-ocean variability such as the North Atlantic Oscillation (NAO) (22). The NAO is known to be strongly coupled to regional sea ice fluctuations (15, 23), and here we find its winter index (22) to be lag-correlated with the following summer minimum ice area and hence the following winter MY ice area (both $r \sim -0.54$, $P \sim 0.02$). Thus the NAO index explains $\sim 25\%$ (r^2) of the MY ice variability.

Further satellite monitoring and analysis of the sea ice cover, together with oceanographic and atmospheric data, are needed to better understand the patterns and processes behind these changes. Moreover, because sea ice parameters are hemispherically integrated measurements, we recommend that quantitative comparisons be made with ice cover output from global coupled climate models in the same manner as global average atmo-

spheric temperature observations, for improved assessment and prediction of global warming in the polar regions.

References and Notes

1. S. Manabe, M. J. Spelman, R. J. Stouffer, *J. Clim.* **5**, 105 (1992).
2. J. F. B. Mitchell, T. C. Johns, J. M. Gregory, S. F. B. Tett, *Nature* **376**, 501 (1995).
3. O. M. Johannessen, M. W. Miles, E. Bjørge, *Nature* **376**, 126 (1995).
4. E. Bjørge, O. M. Johannessen, M. W. Miles, *Geophys. Res. Lett.* **24**, 413 (1997).
5. D. J. Cavalieri, P. Gloersen, C. L. Parkinson, H. J. Zwally, J. C. Comiso, *Science* **278**, 1104 (1997).
6. J. Maslanik, M. C. Serreze, R. G. Barry, *Geophys. Res. Lett.* **23**, 1677 (1996). A comprehensive spatiotemporal analysis of satellite data from 1978 to 1996 revealed some of the greatest decreases ($>20\%$) to be in the summer ice cover over large parts of the East Siberian and Kara seas [C. L. Parkinson, D. J. Cavalieri, P. Gloersen, H. J. Zwally, J. C. Comiso, *J. Geophys. Res.* **104**, 20,837 (1999)].
7. P. Wadhams, *Nature* **345**, 795 (1990). Analysis of data on sea ice thickness from the Greenland Sea and Eurasian Basin acquired from British submarine cruises in 1976 and 1987 showed a 15% decrease. However, the requisite data sets from submarine transects needed to reliably test for changes in overall arctic ice thickness have remained unavailable [P. Wadhams, *J. Geophys. Res.* **102**, 27951 (1997)], although progress is being made; see (19). Additionally, methods of estimating spatially integrated sea ice thickness using spaceborne altimetry appear promising [N. R. Peacock *et al.*, in *Proceedings of the International Geosciences and Remote Sensing Symposium*, Seattle, WA, 6 to 10 July 1998, T. I. Stein, Ed. (IEEE, Piscataway, NJ, 1998), pp. 1964–1966] and may be applied to continuous satellite altimeter data sets made since 1991.
8. J. C. Comiso, *J. Geophys. Res.* **95**, 13,411 (1990).
9. P. Gloersen *et al.*, *Arctic and Antarctic Sea Ice: 1978–1987: Satellite Passive Microwave Observations and Analysis* (NASA, Washington, DC, 1992).
10. T. Grenfell, *J. Geophys. Res.* **97**, 3485 (1992).
11. NORSEX Group, *Science* **220**, 781 (1983).
12. E. Svendsen *et al.*, *J. Geophys. Res.* **88**, 2781 (1983).
13. D. J. Cavalieri, C. L. Parkinson, P. Gloersen, J. C. Comiso, H. J. Zwally, *J. Geophys. Res.* **104**, 15,803 (1999).
14. J. Stroeve, X. Li, J. Maslanik, *Remote Sens. Environ.* **64**, 132 (1998).
15. P. Gloersen and D. J. Cavalieri, *J. Geophys. Res.* **91**, 3913 (1986).
16. R. Kwok and D. A. Rothrock, *J. Geophys. Res.* **104**, 5177 (1999).
17. D. M. Smith, *Geophys. Res. Lett.* **25**, 655 (1998).
18. M. G. McPhee, T. P. Stanton, J. H. Morison, D. G. Martinson, *Geophys. Res. Lett.* **25**, 1729 (1998).
19. D. A. Rothrock, Y. Yu, and G. A. Maykut (*Geophys. Res. Lett.*, in press) compared sea ice draft data acquired by the Scientific Ice Expeditions (SCICEX) program in the mid-1990s with data from 1958 and 1976, finding a mean decrease of 1.3 m (around 40%) in ice thickness over the deep Arctic Ocean, with greater decreases in the eastern and central Arctic than in the western Arctic. These trends are much greater than the ~ 0.1 m reported in (21) and shown in our Fig. 2, although the data sets are not directly comparable. First, the effective ice thickness estimates in Fig. 2 are from 1978–91, so that there is no overlap. Second, the data are from different seasons, and summer and winter trends are not expected a priori to be similar. Third, the 1990s data analyzed by Rothrock *et al.* are from 1993–97, which happens to be a period of unusually large reductions in the summer ice cover, especially in the eastern Arctic, with record low ice minima in 1993 and 1995 (6).
20. A. P. Nagurnyi, V. G. Korostelev, P. A. Abaza, *Bull. Russian Acad. Sci. Phys. Suppl. Phys. Vib.* **58**, 168 (1994).
21. A. P. Nagurnyi, V. G. Korostelev, V. V. Ivanov, *Meteorol. Hydrol.* **3**, 72, (1999) (Russian; English translation available from the Nansen Environmental and Remote Sensing Center).
22. J. W. Hurrell, *Science* **269**, 676 (1995).
23. L. A. Mysak and S. A. Venegas, *Geophys. Res. Lett.* **25**, 3607 (1998).
24. Supported by grants from the European Union's program International Association for the Promotion of Co-operation with Scientists from the Independent States of the Former Soviet Union (INTAS), the Norwegian Research Council's programs International Co-operation: Central and Eastern Europe and Arctic Radiation and Heat, and the Norwegian Space Centre. The satellite data were provided by the National Snow and Ice Data Center in Boulder, CO. We thank A. P. Nagurnyi and H. Sagen for useful discussions on ice thickness retrieval and the two anonymous reviewers for useful comments on the manuscript.

11 August 1999; accepted 27 October 1999

Domain Movement in Gelsolin: A Calcium-Activated Switch

Robert C. Robinson,¹ Marisan Mejillano,² Vincent P. Le,¹ Leslie D. Burtnick,³ Helen L. Yin,² Senyon Choe^{1*}

The actin-binding protein gelsolin is involved in remodeling the actin cytoskeleton during growth-factor signaling, apoptosis, cytokinesis, and cell movement. Calcium-activated gelsolin severs and caps actin filaments. The 3.4 angstrom x-ray structure of the carboxyl-terminal half of gelsolin (G4–G6) in complex with actin reveals the basis for gelsolin activation. Calcium binding induces a conformational rearrangement in which domain G6 is flipped over and translated by about 40 angstroms relative to G4 and G5. The structural reorganization tears apart the continuous β sheet core of G4 and G6. This exposes the actin-binding site on G4, enabling severing and capping of actin filaments to proceed.

The cellular actin scaffold is continuously reorganized in response to a variety of signals. Apoptosis promotes dismantling of the actin cytoskeleton, and growth factor stimulation induces actin filament assembly at the plasma membrane, which leads to cell shape changes and movement. Gelsolin is a calci-

um-activated regulator of these cytoskeletal and motile functions of actin (1). Elevated calcium concentrations activate the filament severing and capping activities of gelsolin, which results in more actin filaments with a shorter average length. The six domains of gelsolin, G1–G6, probably arose through a

REPORTS

sequence of gene triplication followed by gene duplication, resulting in a modular protein in which G4–G6 has an architecture similar to that of G1–G3 (2, 3). We have determined the structure of the complex of G4–G6 bound to actin and calcium at 3.4 Å (Fig. 1A and Table 1). The structure reveals that the binding interface is centered around the interaction of the long helix of G4 with actin. There are also a few contacts between G6 and actin. G5 does not contact actin but forms substantial bridging contacts between G4 and G6,

which have no direct interdomain contacts.

Comparison of the structures of this activated, actin-bound form of G4–G6 with the nonactivated form (4) reveals the structural mechanism of the calcium-controlled latch that regulates actin binding to G4 (Fig. 1B). In calcium-free gelsolin a β sheet runs continuously through the cores of G4 and G6. On binding calcium, this sheet is severed between G4 and G6, which exposes the actin-binding site on G4 (Fig. 1B). During this process G6 rotates about 90° around axes in both the horizontal and vertical planes of Fig. 1B and translates about 40 Å in the vertical

direction to disengage from G4 and establish new contacts with G5. Nonactivated gelsolin has a kink in the long helix of G6 that is required to avert clashes with the long helix of G4 across the core β sheet. The G6 helix is straight in the calcium-activated structure (Fig. 1C) and has a regular α -helical hydrogen-bonding pattern. These additional hydrogen bonds together with the contacts in the new G5–G6 interface and coordination of calcium ions compensate energetically for the disruption of bonds between G6 and G4. Activation causes little change in the orientation of G5 relative to G4. The structure of

¹Structural Biology Laboratory, Salk Institute for Biological Studies, Post Office Box 85800, San Diego, CA 92186–5800, USA. ²Department of Physiology, University of Texas Southwestern Medical Center, 5323 Harry Hines Boulevard, Dallas, TX 75235, USA. ³Department of Chemistry, University of British Columbia Vancouver, BC, Canada V6T 1Z1.

*To whom correspondence should be addressed. E-mail: choe@sbl.salk.edu

Table 1. Summary of data collection and refinement statistics. Diffraction data from a frozen crystal (100 K) were measured with a Fast MAR image plate and 0.97 Å wavelength radiation on beamline 5.0.2, ALS, Berkeley. Reflection data were indexed, integrated, and scaled using DENZO and SCALEPACK (11). Structural analysis was initiated by molecular replacement with an actin monomer (5) as the search model in the program EPMR (12). The solution was unambiguous, and the resulting phase information allowed positioning of G4 (4) in electron density maps in agreement with the G1-actin structure (5). Subsequent electron density maps were of sufficient quality to unequivocally place domains G5 and G6 and to build some linker regions. The model was refined with tight geometric restraints, isotropic B-factors, and a bulk solvent correction in CNS (13) and REFMAC (14), with extra attention given to the free R-factor to monitor the correct progress of refinement. The quality of the final model was assessed in PROCHECK (15). Figures were prepared with the programs MOLSCRIPT (16) and GRASP (17). This model (18, 19) consists of actin residues 5 to 39 and 47 to 375; gelsolin residues 412 to 454, 459 to 704, and 715 to 742; an ATP molecule; and three calcium ions, one of which is entirely coordinated by actin residues, one of which is sandwiched between actin and gelsolin (type 1), and one of which is coordinated by gelsolin alone (type 2).

Space group	P2 ₁ 2 ₁ 2 ₁
Cell	a = 54.5 b = 113.2 c = 158.2 Å $\alpha = \beta = \gamma = 90^\circ$
Asymmetric unit	One complex
Bragg spacing	20.00 to 3.40 Å
Reflections	11329
% completeness	81.0
R_{merge}^*	0.155
R_c^*	24.2
R_{free}^\dagger	30.6
Nonhydrogen atoms	5319
RMS deviation bonds	0.011 Å
RMS deviation angles	2.01°
Mean temperature factor	29.8 Å ²

* $R_{\text{merge}} = (\sum |I - \langle I \rangle| / \sum I)$. $R_c = (\sum |F_o| - |F_c|) / \sum |F_o|$.
†Based on 4% of the data

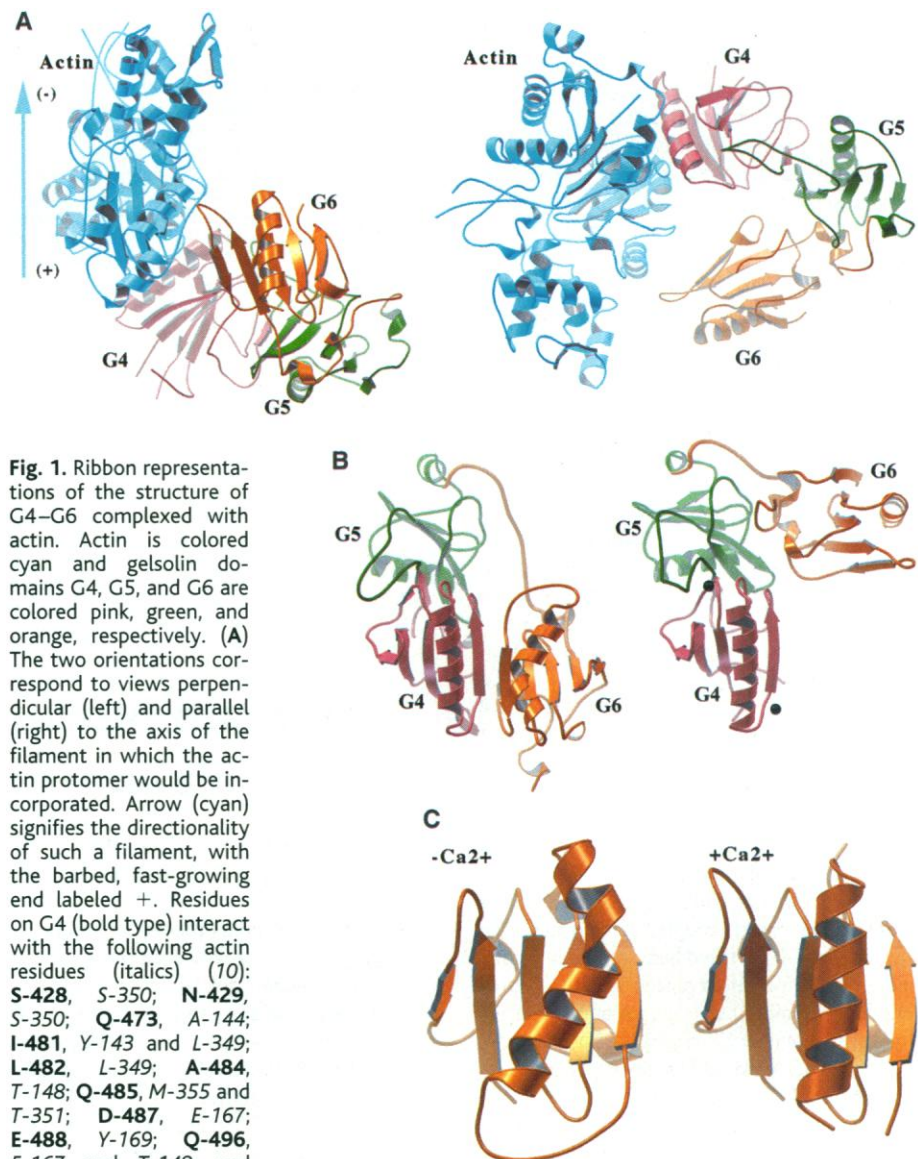


Fig. 1. Ribbon representations of the structure of G4–G6 complexed with actin. Actin is colored cyan and gelsolin domains G4, G5, and G6 are colored pink, green, and orange, respectively. (A) The two orientations correspond to views perpendicular (left) and parallel (right) to the axis of the filament in which the actin protomer would be incorporated. Arrow (cyan) signifies the directionality of such a filament, with the barbed, fast-growing end labeled +. Residues on G4 (bold type) interact with the following actin residues (italics) (10): **S-428**, *S-350*; **N-429**, *S-350*; **Q-473**, *A-144*; **I-481**, *Y-143* and *L-349*; **L-482**, *L-349*; **A-484**, *T-148*; **Q-485**, *M-355* and *T-351*; **D-487**, *E-167*; **E-488**, *Y-169*; **Q-496**, *E-167* and *T-148*; and **R-498**, *R-147* and *N-296*.

Similarly residues on G6 (bold type) form interactions with the following actin residues (italics) **K-648**, *D-311* and *L-221*; **I-649**, *K-315*; **G-650**, *L-22*; and **E-655**, *K-326*. (B) Comparison of the structures of the G4–G6 domains in nonactivated gelsolin (4) (left) and in complex with actin and Ca²⁺ (right). Orientation of G4 in both panels is about the same. The front side of G4 (pink) is the actin-binding site. The far right β strand of G4 tears apart from the far left β strand of G6 upon calcium activation, exposing the actin-binding interface. The two calcium ions are shown as black spheres. (C) (Left) Structure of the nonactivated G6 (4); (right) actin-bound form of G6 in a similar orientation.

REPORTS

the complexed actin, which is also bound to an adenosine triphosphate (ATP) molecule and a calcium ion, is not significantly different from the structure in the G1-actin complex reported by McLaughlin *et al.* (5).

Because of the gene duplication that gen-

erated the six-domain gelsolin from a three-domain precursor, and the consequent similarity in the tertiary structures of G1–G3 and G4–G6 (4), it is likely that the two halves of gelsolin share many functional properties. For example, of the 11 residues that form

direct interactions with actin in G1 and G4, 6 are identical and 4 are conservatively substituted (Fig. 2A). The one difference, Phe⁴⁹ in G1 compared with Ser⁴²⁸ in G4, does not affect the binding interface as these residues interact with actin residue Ser³⁵⁰ through

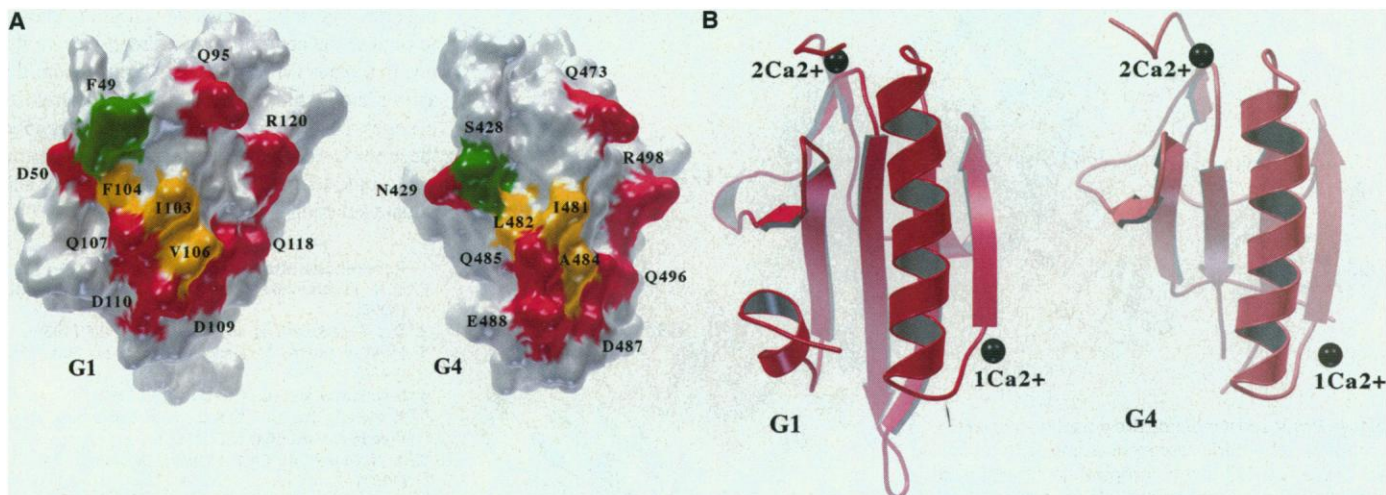


Fig. 2. Comparison of the G1 and G4 actin-binding sites. (A) Surface representations of G1 and G4 detailing residues at the actin–gelsolin interface. Charged residues, hydrophobic residues, and nonconserved residues are colored red, yellow, and green, respectively. (B) Actin-bound

forms of G1 (5) (red) and G4 (pink) in about the same orientation as in (A) are shown as schematic representations. Bound calcium ions are shown as black spheres. Type 1 calcium ions are labeled 1Ca²⁺ and type 2 are labeled 2Ca²⁺.

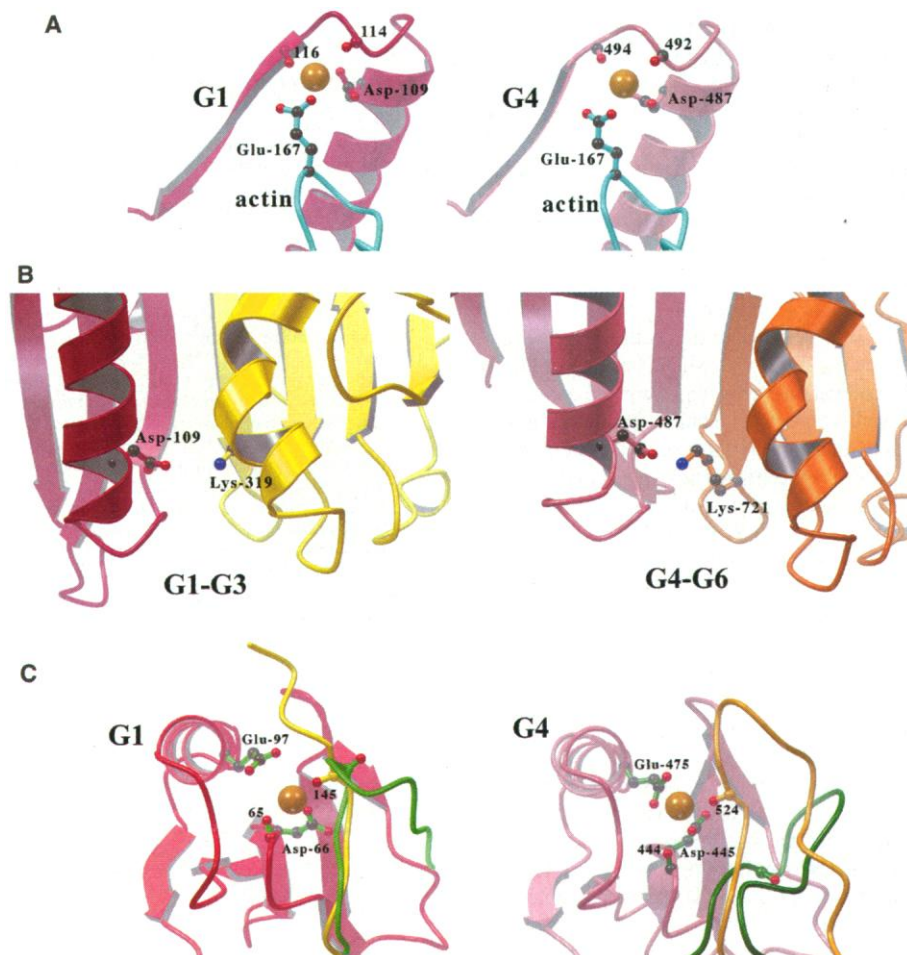


Fig. 3. Calcium-binding sites of gelsolin. (A) Coordination of the sandwiched type 1 calcium ions (gold) in G1 (5) (left) (red) and G4 (right) (pink). Actin is cyan and calcium-binding residues are colored and labeled accordingly. (B) Positions of calcium-binding residues from (A), Asp¹⁰⁹ and Asp⁴⁸⁷, in nonactivated gelsolin (4). Asp¹⁰⁹ in domain G1 (red) forms a salt bridge with Lys³¹⁹ in domain G3 (yellow) (left). Similarly Asp⁴⁸⁷ from domain G4 (pink) forms a salt bridge with Lys⁷²¹ in domain G6 (orange) (right). (C) Type 2 calcium ions are coordinated entirely by gelsolin. (Left) Calcium ion (gold) coordinated by G1 (red). Chain trace of residues 140 to 150 for nonactivated gelsolin (4) (light green) and activated gelsolin (5) (yellow) are included for comparison. The carbonyl group of residue 145 rotates by 180° to coordinate this calcium. (Right) Type 2 calcium ion coordinated by G4 (pink). Backbone trace of residues 519 to 535 from the nonactivated form of gelsolin (4) (dark green) and from activated gelsolin (gold) are also included for comparison.

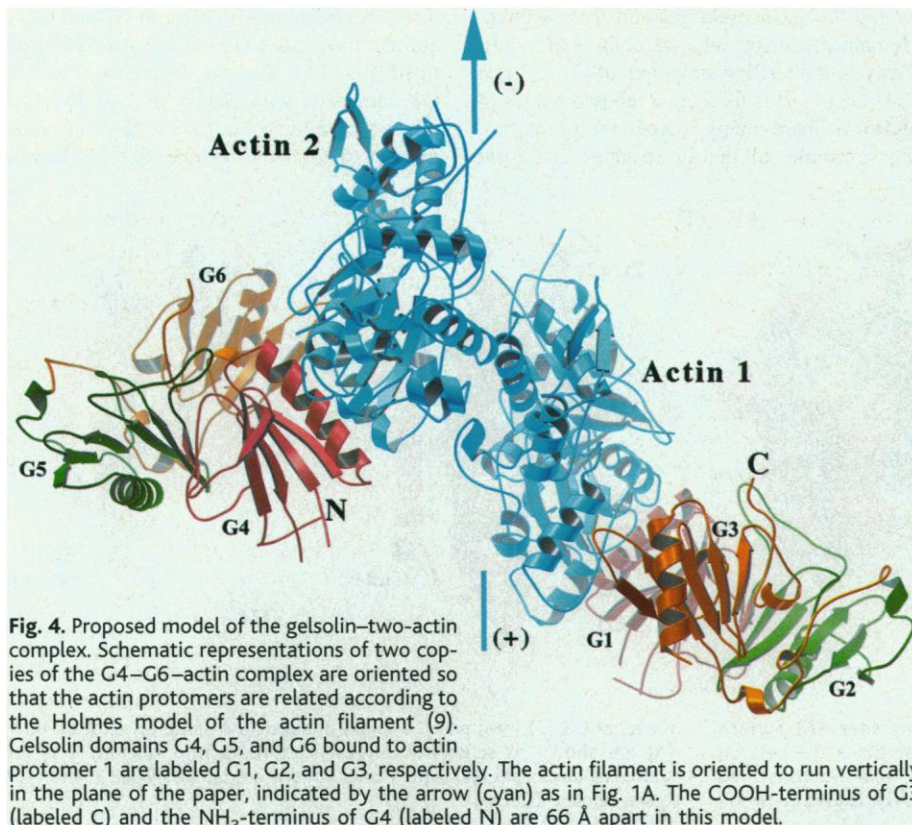


Fig. 4. Proposed model of the gelsolin-two-actin complex. Schematic representations of two copies of the G4–G6–actin complex are oriented so that the actin protomers are related according to the Holmes model of the actin filament (9). Gelsolin domains G4, G5, and G6 bound to actin protomer 1 are labeled G1, G2, and G3, respectively. The actin filament is oriented to run vertically in the plane of the paper, indicated by the arrow (cyan) as in Fig. 1A. The COOH-terminus of G3 (labeled C) and the NH₂-terminus of G4 (labeled N) are 66 Å apart in this model.

their backbone atoms. The two halves of gelsolin also display some divergent properties, exemplified by domain G2 harboring an F-actin-binding activity (6), whereas G5, the homologous domain in the carboxyl-terminal half, does not bind to actin.

There are two sites of Ca²⁺ coordination in the actin-complexed G1 domain (5), and Ca²⁺ occupies the corresponding sites in the G4 domain in the G4–G6 complex with actin (Fig. 2B). The two type 1 calcium-binding sites (Fig. 3A) are formed at the interface between G1 or G4 and the actin residue Glu¹⁶⁷. Gelsolin residues involved in calcium binding are Asp¹⁰⁹ and the carbonyl groups of residues 114 and 116 in G1 and Asp⁴⁸⁷ and the carbonyl groups of residues 492 and 494 in G4. In nonactivated gelsolin Asp¹⁰⁹ and Asp⁴⁸⁷ both form a salt bridge with a lysine residue across the G1–G3 or G4–G6 β sheets (Fig. 3B). Calcium binding at either Asp¹⁰⁹ or Asp⁴⁸⁷ is incompatible with these salt bridges and could facilitate severing of the G1–G3 and G4–G6 β sheets. The two type 2 calcium-binding sites (Fig. 3C) are entirely contained within G1 and G4. Coordination is through the conserved residues Asp⁶⁶ and Glu⁹⁷ from G1 and Asp⁴⁴⁵ and Glu⁴⁷⁵ from G4. We have suggested previously (4) that, during gelsolin binding to an actin filament, calcium binding at the type 2 site in G1 may cause reorienting of G2 so that G2 can contact the actin protomer that is next along the filament axis relative to the G1-bound protomer. This would trap the calcium in an EGTA-resis-

tant coordination (7). Calcium binding at the type 2 site in G4 does not induce a dramatic repositioning of G5, functionally consistent with G5 not binding to actin. Instead the greater length of the G4–G5 loop relative to the G1–G2 loop can accommodate calcium coordination without domain rearrangement. Calcium binding at this K_d-2 μM (8) type 2 site on G4 is EGTA-reversible and may be largely redundant, being a carryover from the most recent gene duplication event in gelsolin's history. A fifth calcium-binding site, with a K_d of 0.2 μM, exists in G5–G6 (8), which, because of affinity considerations, may represent the most functionally important calcium-binding site in G4–G6. Unfortunately this site could not be identified in the electron-density maps and therefore may reside in regions of poor electron density (residues 626 to 632, 707 to 713, or 742 to 755).

The structural similarities between the two halves of gelsolin imply that a calcium-activated switch mechanism, analogous to that discussed for G4–G6, operates to dissociate the continuous β sheet between G1 and G3 and unmask the actin-binding site on G1. We have generated a model in which the G1–G3 and G4–G6 halves of whole gelsolin are bound to two adjacent actin protomers in the Holmes (9) presentation of filamentous actin (Fig. 4). In this model, the 46-amino acid linker between G3 and G4 is sufficiently long to span the 66 Å gap between G3 and G4. A less probable model, with G4–G6 positioned on the actin subunit directly below actin 2 in Fig. 4, is more steri-

cally hampered and has a greater separation between G3 and G4 (93 Å). The model in Fig. 4 may represent the stable complex of gelsolin with two isolated actin monomers. From this model, we can infer that further structural changes in gelsolin must occur during the severing process. In particular, the third actin-binding site of gelsolin resides on G2; G2 is known to bind to the actin protomer directly above the one that binds G1 (5, 6). G2 is remote from the actin filament in the model in Fig. 4. Therefore, changes in the structure of G1–G3, beyond those we have suggested, must occur to permit G2 to bind to the side of an actin filament and initiate severing.

References and Notes

1. D. J. Kwiatkowski, *Curr. Opin. Cell Biol.* **11**, 103 (1999).
2. D. J. Kwiatkowski *et al.*, *Nature* **323**, 455 (1986).
3. M. Way and A. G. Weeds, *J. Mol. Biol.* **203**, 1127 (1988).
4. L. D. Burtnick *et al.*, *Cell* **90**, 661 (1997).
5. P. McLaughlin, J. T. Gooch, H.-G. Mannherz, A. G. Weeds, *Nature* **364**, 685 (1993).
6. A. McGough, W. Chiu, M. Way, *Biophys. J.* **74**, 764 (1998).
7. A. G. Weeds *et al.*, *FEBS Lett.* **360**, 227 (1995).
8. B. Pope, S. Maciver, A. Weeds, *Biochemistry* **34**, 1583 (1995).
9. K. C. Holmes, D. Popp, W. Gebhard, W. Kabsch, *Nature* **347**, 44 (1990).
10. Amino acid residues are abbreviated as follows: A, Ala; C, Cys; D, Asp; E, Glu; F, Phe; G, Gly; H, His; I, Ile; K, Lys; L, Leu; M, Met; N, Asn; P, Pro; Q, Gln; R, Arg; S, Ser; T, Thr; V, Val; W, Trp; Y, Tyr.
11. Z. Otwinowski, in *Data Collection and Processing* L. Sawyer, N. Issacs, S. Bailey, Eds. (SERC Daresbury Laboratory, Warrington, 1993), pp. 56–62.
12. C. R. Kissinger, D. K. Gehlaar, D. B. Fogel, *Acta Crystallogr.* **D55**, 484 (1999).
13. A. T. Brünger *et al.*, *Acta Crystallogr.* **D54**, 905 (1998).
14. CCP4, *Acta Crystallogr.* **D55**, 760 (1994).
15. R. J. Laskowski, M. W. MacArthur, D. S. Moss, J. M. Thornton, *J. Appl. Crystallogr.* **26**, 283 (1993).
16. P. Kraulis, *J. Appl. Crystallogr.* **24**, 946 (1991).
17. A. Nicholls and B. Honig, *J. Comp. Chem.* **12**, 435 (1991).
18. An expression vector was constructed by the polymerase chain reaction to generate a DNA fragment encoding domains G4–G6 of human plasma gelsolin (residues 407 to 755) [K. M. Lin, E. Wengieme, P. J. Lu, C. S. Chen, H. L. Yin, *J. Mol. Biol.* **272**, 20443 (1997)]. G4–G6 was expressed as a glutathione S-transferase fusion protein and released from a glutathione column by thrombin. Actin was purified from rabbit muscle acetone powder [J. A. Spudich and S. Watt, *J. Mol. Biol.* **246**, 4866 (1971)]. Actin and G4–G6 were mixed in a 1:1 ratio and the complex was separated on a Superdex 200 (Pharmacia) gel filtration column in 5 mM tris-HCl (pH 8.0), 0.2 mM ATP, 0.1 mM CaCl₂, 0.5 mM dithiothreitol. Crystals were grown at 4°C from a protein sample (10 mg/ml) combined in a 1:1 ratio with a well solution consisting of 10% PEG 8000, 20% glycerol, and 100 mM Hepes (pH 7.5).
19. Atomic coordinates have been deposited in the Protein Data Bank (accession number 1DB0).
20. Supported by grants from the Heart and Stroke Foundation of British Columbia and Yukon (L.D.B.), National Institutes of Health (S.C., H.L.Y.), the American Heart Association (Texas) (H.L.Y.), and the Pioneer Fund and Hoffmann Foundation (R.C.R.). We thank W. Kwiatkowski for computing expertise and help with figure preparation, the ALS synchrotron source for help with data collection, S. Almo for supplying coordinates for yeast actin, and L. Blanchoin for gifts of actin.

8 September 1999; accepted 2 November 1999